Scaffolding of NLRP3 on osmotically swollen vesicles but not intermediate filaments promotes inflammasome assembly

Guillermo de Paz Linares[1,2], Jan Mossemann[1], Blayne Sayed[1,3], and Spencer A. Freeman[1,2*]

[1]Program in Cell Biology, Hospital for Sick Children, Toronto, Ontario M5G 0A4, Canada

[2]Department of Biochemistry and the [3]Institute of Medical Science, University of Toronto, Toronto, ON M5S 1A8, Canada.

*Corresponding author: spencer.freeman@sickkids.ca

Key words: vimentin, membrane tension, V-ATPase, LAMP-1, PI(4)P, PI(3,5)P2, PI(3)P, ischemia reperfusion injury

Abstract

Inflammasomes are nucleated by receptors that become activated upon cellular stresses including ionic dyshomeostasis. Rather than forming in the cytosol, recent evidence suggests that inflammasomes are nucleated at specific sites in the cell including on cytoskeletal polymers and the membrane surfaces of organelles. The NLRP3 inflammasome, which is formed upon the loss of cytosolic K^+, had been proposed to form on intermediate filaments as well as on vesicles derived from the trans-Golgi network and endosomes. To determine the necessary requirement of either mechanism, we used vimentin knockout macrophages which do not have intermediate filaments and compared the formation and function of NLRP3 inflammasomes. We report that vimentin was dispensable for the activation of caspase-1, IL-β cleavage and release, and the inflammatory responses in mice which are attributed to the inflammasome. Instead, NLRP3 was found on osmotically swollen PI4P- and LAMP1-positive compartments. These results provide clarification to the two models for NLRP3 inflammasome formation, demonstrating that intermediate filaments are not required, which contrasts with select previous literature. The results also suggest that NLRP3 may be activated by signals coincident with PI4P, including high membrane tension on vesicular compartments.

Introduction

Inflammasomes are supramolecular organizing centres (SMOCs) that assemble in response to diverse threats to cell and tissue homeostasis. Such threats often involve the loss of membrane integrity and/or the breach of the cytosol by microbial-associated molecules (Greaney, Leppla, and Moayeri 2015). The damage that triggers inflammasome activation ultimately leads to cytokine processing and release, which in turn promotes inflammatory cascades and the recruitment of immune cells. Inflammasome assembly is a stepwise process which begins with a transcriptional priming that upregulates expression of its necessary components. This is followed by the sensing of intracellular perturbances via cytosolic pattern recognition receptors (PRR) and their recruitment of the effector protease, caspase-1. Once concentrated, caspase-1 initiates self-cleavage, activation, and subsequent processing of inflammatory mediators including IL-1β and gasdermin D (Brough and Rothwell 2007; He et al. 2015). The NLRP3 inflammasome, which has been extensively studied, is activated in response to insults that ostensibly cause the collapse of the Na^+:K^+ gradient between the cytosol and the external medium (Muñoz-Planillo et al. 2013; Perregaux and Gabel 1994; Mangan et al. 2024). Its activation is therefore caused by disruption to plasma membrane permeability by diverse bacterial toxins and damage-associated molecular patterns like extracellular ATP (Franchi and Núñez 2008; Perregaux and Gabel 1994; Laliberte, Eggler, and Gabel 1999). Additionally, the accumulation of damaging particulates including alum and monosodium urate crystals (MSU) in the endocytic pathway triggers NLRP3 inflammasome activation (Hanfen Li et al. 2008; Hornung et al. 2008; Martinon et al. 2006), though mechanisms in this case are less clear (Mangan et al. 2024). Pharmacology aimed at inhibiting NLRP3 has shown enormous potential at mitigating conditions with an underlying chronic inflammatory etiology (Hao Li et al. 2022).

Despite the clear relevance of NLRP3 inflammasome nucleation, recent studies on the location of NLRP3 inflammasome assembly have been seemingly at odds with one another. One report by dos Santos et al. (dos Santos et al. 2015), argued that vimentin-based

77 intermediate filaments are required for the assembly of the NLRP3 inflammasome in primary
78 murine macrophages. NLRP3 was found to colocalize and co-sediment with vimentin and the
79 loss of vimentin prevented inflammasome assembly and inflammation. This would seem to be in
80 contrast to other subsequent reports (Chen and Chen 2018; Zhang et al. 2023; Schmacke et al.
81 2022) that have found that NLRP3 begins to aggregate on phosphatidylinositol-4-phosphate
82 (PI4P)-enriched intracellular vesicles. Structurally, PI4P is thought to interact with a stretch of
83 positively charged residues found on NLRP3. This motif, known as the polybasic region, was
84 essential in mediating the initial assembly of the NLRP3 inflammasome in cell lines. Thus, both
85 models appear to be diametrically opposed, since vimentin is not known to be required for any
86 PI4P-mediated processes.

87 In this report, we revisit the role of intermediate filaments in the inflammatory response
88 of macrophages, where cytosolic intermediate filaments are solely comprised of vimentin, to
89 NLRP3-activating stimuli. Despite reports of vimentin knockout (*Vim*$^{-/-}$) mice as being protected
90 against a plethora of inflammatory insults (Jiang et al. 2012; dos Santos et al. 2015; Mor-Vaknin
91 et al. 2013; Håversen et al. 2018), we do not find a role for vimentin in the nucleation of the
92 NLRP3 inflammasome nor the subsequent release of inflammatory cytokines from
93 macrophages. Supporting this, we found that *Vim*$^{-/-}$ mice were not protected against
94 inflammation in an *in vivo* model of liver ischemia reperfusion injury, an NLRP3-dependent
95 process. Therefore, it appears that the protective effects observed in *Vim*$^{-/-}$ mice are attributed to
96 functions independent of NLRP3. Instead, we find that NLRP3 is recruited to PI4P- and LAMP-1
97 containing, osmotically-swollen vesicles that appear after collapsing the K^+ gradient. NLRP3
98 became soluble upon relieving hydrostatic tension of the organelles. This would suggest
99 coincident detection of NLRP3 for lipids and biophysical features of the membrane to trigger
100 inflammasome formation.

101

102 **Results**

103 *ASC specks form independently of vimentin*

104 To test the proposed requirement for vimentin filaments in the nucleation of the NLRP3
105 inflammasomes, we derived primary macrophages from the bone marrow of *Vim*$^{-/-}$ mice. Our
106 bone marrow-derived macrophages (BMDM) did not express vimentin as judged by western
107 blotting (**Fig 1A**) and immunofluorescence (**Fig 1B**). NLRP3-mediated pyroptosis is triggered by
108 the depletion of intracellular [K^+], including for primary macrophages (Muñoz-Planillo et al.
109 2013). Experimentally, this is most conveniently achieved with nigericin, a K^+ ionophore.
110 Alternatively, we also used ATP, which engages purinergic receptors to cause their
111 multimerization and formation of a non-selective pore that conducts K^+ down its concentration
112 gradient, i.e. out of the cell (Pelegrin and Surprenant 2006). We used nigericin and ATP at
113 standard concentrations and times known to instigate NLRP3 inflammasome formation in a
114 manner dependent on net K^+-efflux (Perregaux and Gabel 1994; Muñoz-Planillo et al. 2013).
115 Using atomic absorption spectroscopy, we found that the loss of intracellular K^+ upon the
116 addition of nigericin or ATP was not different between wt and *Vim*$^{-/-}$ BMDM, as expected **(Fig.**
117 **1C)**. Therefore, any differences in NLRP3 inflammasome activation would not be caused by
118 protection against intracellular [K^+] depletion in *Vim*$^{-/-}$ BMDM.

119 Next, we visualized K^+ efflux-dependent ASC speck formation in lipopolysaccharide
120 (LPS)-primed BMDM, which upregulates the expression of NLRP3 (Bauernfeind et al. 2009).
121 ASC is a critical adaptor that enables the recruitment of caspase-1 to NLRP3 and its
122 subsequent activation (Man et al. 2014). We stained endogenous ASC following nigericin or ATP
123 treatment and, surprisingly, found no difference in the incidence of ASC-speck positive BMDM
124 between wt and *Vim*$^{-/-}$ cells **(Fig. 1D,E).** Even more remarkable, when analyzing images using a
125 Pearson's coefficient, we found there to be no correlation between the localization of vimentin
126 intermediate filaments and ASC specks following NLRP3 inflammasome activation **(Fig. 1F,G)**.
127 This is despite the fact that the intermediate filaments persisted in activated cells. Altogether,

128 these observations would seem to indicate that the assembly of the NLRP3 inflammasome is
129 not dependent on the presence of vimentin intermediate filaments.
130
131 *Vimentin is not required for NLRP3-mediated pyroptosis*
132 Once the NLRP3 inflammasome forms, active caspase-1 then cleaves the protein
133 gasdermin D (GSDMD) and pro-IL-1β. Subsequently, the N-terminus of GSDMD inserts into the
134 plasma membrane to form a pore that allows for the passage and release of the processed
135 (mature) IL-1β (Evavold et al. 2018). The involvement of intermediate filaments in GSDMD pore
136 assembly was not assessed in previous studies; conceivably, if vimentin controlled the release
137 of proinflammatory mediators it would explain some results in mice in which KOs are protected
138 from inflammation (Jiang et al. 2012; Håversen et al. 2018; Mor-Vaknin et al. 2013; dos Santos
139 et al. 2015). We treated LPS-primed wt and *Vim*$^{-/-}$ BMDM with nigericin along with propidium
140 iodide (PI) in order to identify potential differences in the rate of plasma membrane
141 permeabilization **(Fig. 2A,B)**. However, we did not see appreciable differences between the
142 vimentin KO macrophages when compared to their wt counterparts.
143 Sustained GSDMD pore activity eventually leads to an irreversible form of lytic cell death
144 known as pyroptosis that further promotes IL-1β release into the interstitium (Fink and Cookson
145 2006; He et al. 2015). Thus, we investigated whether the absence of vimentin in BMDM could
146 prevent or stagnate pyroptosis by measuring the release of lactate dehydrogenase (LDH). In
147 addition to instigating pyroptosis with nigericin or ATP, we also employed alum and MSU crystals
148 to trigger the process. As shown by this assay, nigericin, ATP, alum, and MSU induce lytic cell
149 death in both wt and *Vim*$^{-/-}$ LPS-primed BMDM **(Fig. 2C)**. Moreover, the amount of LDH release
150 in *Vim*$^{-/-}$ BMDM was not significantly different than in wt BMDM irrespective of the NLRP3
151 inflammasome activator used. Based on our results, we conclude that *Vim*$^{-/-}$ BMDM are not
152 protected against pyroptotic cell death.

153

154 *Vimentin is not required for NLRP3-dependent cleavage and release of caspase-1 nor IL-1β*

155 During pyroptosis, caspase-1 activation precedes the cleavage of IL-1β and has been
156 reported to exit the cell as an active protease following cell rupture (Laliberte, Eggler, and Gabel
157 1999). Indeed, we found cleaved (i.e., active) caspase-1 in the supernatants of LPS-primed
158 BMDM that were treated with either nigericin or ATP **(Fig. 3A)**. Remarkably, we saw that *Vim*$^{-/-}$
159 BMDM were activating and releasing comparable amounts of caspase-1 compared to their wt
160 BMDM counterparts upon pyroptotic stimuli **(Fig. 3A,B)**.

161 Ultimately, IL-1β is a major effector cytokine that results in the propagation of
162 inflammatory responses. We found that BMDM derived from the *Vim*$^{-/-}$ mice had no impairment
163 in the upregulation of pro-IL-1β upon LPS stimulation **(Fig. 3C)** and released similar levels of
164 active IL-1β into the supernatant after stimulation with either nigericin or ATP **(Fig 3C)**.
165 Furthermore, we saw no difference in the mature IL-1β concentration found in the extracellular
166 medium of LPS-primed BMDM treated with nigericin or ATP or upon lysosomal stress (i.e., alum
167 or MSU) **(Fig. 3D)**. Overall, we did not observe any impairment in capase-1 and IL-1β
168 processing and release from *Vim*$^{-/-}$ BMDM.

169

170 *Vim*$^{-/-}$ *mice are not protected against hepatic ischemia/reperfusion injury*

171 Despite our *in vitro* observations, there is a plethora of studies reporting that *Vim*$^{-/-}$ mice
172 display reduced tissue damage upon numerous inflammatory stimuli (Jiang et al. 2012;
173 Håversen et al. 2018; Mor-Vaknin et al. 2013). In fact, others have reported that *Vim*$^{-/-}$ mice are
174 protected against cerebral ischemia/reperfusion injury (IRI) (Jiang et al. 2012). Thus, we probed
175 whether this protection translated to a hepatic IRI model, which is reportedly mediated, at least
176 in part, by NLRP3 (Jaeschke 2003; Jiménez-Castro et al. 2019; Zhu et al. 2011). Following 1 h
177 of ischemia and 6 h blood reperfusion, we collected samples from mice to look at different

178 aspects of inflammatory injury. First, we did not observe any cohort differences in plasma levels
179 of liver enzymes alanine aminotransferase (ALT) and aspartate aminotransferase (AST) **(Fig.**
180 **4A,B)**, indicating that liver damage was not ameliorated in the absence of vimentin. Our
181 histological analyses in which we categorized the percentage of necrotic tissue found in the
182 livers after surgery **(***see demarcated yellow areas in* **Fig. 4C)** revealed that, surprisingly, *Vim*$^{-/-}$
183 livers were more necrotic compared to wt **(Fig. 4D)**. Based on these observations, we conclude
184 that the absence of vimentin does not confer a protective effect against the inflammatory
185 damage associated with hepatic IRI.
186
187 *K^+ efflux causes swelling of PI4P-positive membrane-bound organelles to promote NLRP3*
188 *nucleation.*
189 As previously mentioned, opposing views about NLRP3 scaffolding suggest that
190 inflammasome nucleation initiates on PI4P-enriched structures (Schmacke et al. 2022; Chen
191 and Chen 2018; Zhang et al. 2023). It is therefore rather peculiar that NLRP3 was also reported
192 to recognize other phosphoinositides *in vitro*, namely PI3P and PI(3,5)P_2, though these
193 interactions were not validated using any live cell models (Chen and Chen 2018). We expressed
194 an mCherry-NLRP3 fusion protein in HeLa cells, first noting that nigericin treatment resulted in
195 its translocation to vesicular structures **(Fig. 5A and Supplemental movie 1)**. We then
196 reperformed these experiments, co-expressing mCherry-NLRP3 together with biosensors for
197 phosphoinositides **(Fig. 5B)**. We used Statistical Object Distance Analysis (SODA) to determine
198 coincidence of the signals, which provides statistical maps of the assemblies in a population of
199 objects by using morphology and distance separating objects (Lagache et al. 2018). By this
200 method, we identified objects that were significantly coupled within approximately 500 nm. As
201 shown in Figure 5B and quantified in Figure 5C, we noted much less association between
202 NLRP3 and the PI3P (2xFyve-GFP) or PI(3,5)P_2 (SnxA-GFP) probes when compared with PI4P

203 (P4M-GFP) **(Fig. 5C)**. These data would seem to corroborate the finding that NLRP3 assembly
204 is spatially organized around sites of enriched with PI4P.
205 Based on the swollen appearance of the NLRP3-positive compartments that appeared
206 after nigericin treatment, we questioned whether (osmotic) swelling of these vesicular structures
207 was necessary for NLRP3 nucleation. In order to test this, we forcibly extracted water from
208 nigericin-treated cells, and these organelles, using acute treatment with hypertonic solutions**.**
209 Consistently, we observed that NLRP3 dissociated from the vesicles and became largely
210 soluble after this treatment **(Fig. 5D)**. The identity of the swollen vesicles was then interrogated.
211 We noted no overlap between NLRP3 and EEA1 or Rab5 (not shown), but did note appreciable
212 localization of LAMP-1 in the NLRP3 positive vesicles (**Fig 5E**). The LAMP-1 expression on
213 these vesicles was lower than neighbouring NLRP3-negative structures. This would suggest
214 either dilution of LAMP-1 owed to swelling or that these represent a hybrid or intermediary
215 compartment, perhaps involving the trans Golgi. Swelling of lysosomes and the TGN in other
216 settings requires the activity of the V-ATPase. We therefore disrupted the activity of the V-
217 ATPase using concanamycin A, which prevented vesicular swelling upon nigericin treatment
218 **(Fig. 5F)**. The same treatment largely prevented NLRP3 targeting to membrane-bound
219 organelles (**Fig. 5F**). Taken together, it would seem likely that vesicular swelling, driven by the
220 V-ATPase, is necessary for K^+-efflux driven nucleation of NLRP3.
221
222 **Discussion**
223 NLRP3 plays a crucial role in innate immunity by acting as a sensor of intracellular
224 dyshomeostasis. Potassium efflux, indicative of lost plasma membrane integrity or inhibition of
225 the Na/K-ATPase has been shown to be a canonical trigger of NLRP3 inflammasome assembly
226 (Muñoz-Planillo et al. 2013). Solid particles and crystals can also activate the NLRP3
227 inflammasome by causing stress and dysregulation along the endocytic pathway (Hanfen Li et
228 al. 2008; Hari et al. 2014; Groß et al. 2016; Hornung et al. 2008). In this study, we demonstrate

229 that vimentin is dispensable for K^+-efflux- and solid particle-mediated inflammasome assembly,
230 IL-1β processing, and pyroptosis in BMDM, contrary to previous findings (dos Santos et al.
231 2015). *In vivo* assessments of *Vim*$^{-/-}$ mice subjected to hepatic IRI paint a similar picture to our
232 *in vitro* data. Liver IRI is reportedly mediated by, amongst other proteins, NLRP3 and GSDMD
233 (Zhu et al. 2011; Jiménez-Castro et al. 2019; Wu et al. 2022; J. Li et al. 2020), which are
234 seemingly unaffected by the absence of vimentin filaments. Yet, there is an abundance of
235 studies where *Vim*$^{-/-}$ mice are protected against inflammation caused by either sterile or
236 pathogenic injury (Mor-Vaknin et al. 2013; Jiang et al. 2012; Eckes et al. 2000; Håversen et al.
237 2018). Explanations for these phenomena vary from study to study, with no seemingly
238 underlying common mechanism behind it. Impaired immune cell migration and infiltration to
239 inflamed tissues could be an underlying feature (Barberis et al. 2009; Battaglia et al. 2018;
240 Ivaska et al. 2007; Nieminen et al. 2006). Interestingly, we observed the opposite in our mice,
241 whereby the absence of vimentin conferred a worse outcome as measured by percent necrosis
242 and ALT/AST plasma levels. As such, involvement of vimentin during inflammatory injuries
243 appears dependent on the injury site and the type/duration of damage. Though we only looked
244 at liver injury, how intermediate filaments in immune cells feature in other models for IRI in
245 different organs warrant further investigation.
246 In line with other studies (Zhang et al. 2023; Chen and Chen 2018), our data show that
247 the formation of an NLRP3 inflammasome begins at vesicular sites with enriched PI4P following
248 stimuli (e.g., nigericin). Due to the un-primed nature of HeLa cells, nigericin treatment did not
249 induce cell death and allowed for a better model to overexpress and observe the initial NLRP3
250 aggregation. Despite the reported ability for NLRP3 to recognize other phosphoinositides (i.e.,
251 PI3P and PI(3,5)P_2) (Chen and Chen 2018), we found that NLRP3 associated significantly less
252 with the PI3P 2xFyve-GFP and recently developed SnxA-GFP PI(3,5)P_2 biosensor (Vines et al.
253 2023). Therefore, it is reasonable to conclude that PI4P is a bona fide scaffold for NLRP3
254 inflammasome assembly. Interestingly, PI4P has recently been shown to mediate important

255 immune processes pertaining to intracellular danger signals. The cGAS-STING pathway,
256 responsible for sensing cytosolic DNA, was shown to be affected by changes to the intracellular
257 pool of Golgi-PI4P and its associated kinase, PI4KB (Fang et al. 2023; Luteijn et al. 2024). This
258 suggests that the exposure of PI4P plays a broad and diverse role in triggering innate immune
259 responses. It would also seem to suggest that other mediators must be involved.

260 Under normal conditions, the majority of PI4P in cells is located at the Golgi apparatus
261 and the plasma membrane, as tightly regulated by lipid kinases and phosphatases (Tan and Brill
262 2014). NLRP3 does not initiate nucleation prior to K^+ efflux, even with large amounts of PI4P in
263 one site (i.e. at the Golgi). Likewise, NLRP3 upregulation by TLR4 signalling does not alone
264 trigger inflammasome assembly, (Bauernfeind et al. 2009; Kelley et al. 2019), even though PI4P
265 is present and available to bind. This would indeed suggest that PI4P is required but not
266 sufficient to initiate inflammasome formation. While changes in the extracellular osmolarity have
267 been described as a trigger for inflammasome assembly, explanations for this mechanism vary
268 from study to study (Schorn et al. 2011; Mayes-Hopfinger et al. 2021; Compan et al. 2012).
269 Organelle swelling, as induced by hypotonic solutions and K^+-efflux, may be an important
270 parameter necessary for NLRP3 aggregation. In support of this idea, forcibly reducing vesicular
271 swelling leads to the solubilization of NLRP3 away from sites of high PI4P content. Whether or
272 not membrane tension generated on PI4P-enriched swollen organelles arranges the PI4P or
273 exposes determinants otherwise hidden in the bilayer should be tested.

274 While K^+-efflux is a common trigger of the NLRP3 inflammasome, lysosome-damaging
275 stimuli such as alum, monosodium urate crystals, and silica particles have also been reported to
276 trigger its assembly (Hari et al. 2014; Groß et al. 2016). So far, the connection between
277 lysosome-damaging stimuli and the collapse of the K^+ gradient between the cytosol and the
278 extracellular fluid is not known. We observe that K^+-efflux promotes swelling of LAMP1-positive
279 structures, indicating a connection between the loss of cytosolic cation gradients and membrane

280 traffic defects. We also see NLRP3 associated with these swollen compartments, which posits a
281 role for defects in TGN-lysosome traffic in NLRP3 nucleation.
282 Disruption of lysosomal function by bafilomycin A was reported to promote NLRP3
283 inflammasome activation in LPS-primed monocytes. Yet, we saw that treatment of cells with
284 Concanamycin A, a more specific V-ATPase inhibitor, prevents the association of NLRP3 with
285 swollen vesicles (Yu et al. 2021). Of note, we treated our cells with Concanamycin A prior to
286 nigericin addition, suggesting that it might only attenuate NLRP3 aggregation prior to K^+-efflux-
287 induced lysosomal swelling. Hypothetically, a possible explanation is that the initial organellar
288 swelling required for NLRP3 aggregation at LAMP-1 compartments is V-ATPase dependent.
289 Altogether, an extensive understanding of the relationship between V-ATPase-mediated
290 lysosomal swelling and NLRP3 nucleation kinetics remains of critical importance.
291
292 **Methods and materials**
293 *Animals*
294 *Vim*$^{-/-}$ (129S-*Vim*^{tm1Cba}/MesDmarkJ, stock #025692) and wt 129S1 mice (129S1/SvImJ,
295 strain #002448) were obtained from Jackson Labs as previously described (Colucci-Guyon et al.
296 1994). wt mice from Jackson Labs (strain #000664) were used where indicated. All procedures
297 were approved by the Animal Care Committee at the Hospital for Sick Children and were
298 performed in accordance with regulations from the Animals for Research Act of Ontario and the
299 Canadian Council on Animal Care. Mice were kept at the Animal Facility in the Peter Gilgan
300 Centre for Research and Learning.
301
302 *Liver ischemia/reperfusion surgery*
303 Mixed-sex cohorts of 8- to 12-week-old Vimentin knockout and wt (C57Bl/6) control mice
304 were used in a 70% segmental warm ischemia-reperfusion model (Selzner et al. 2003). In brief,
305 a sagittal midline laparotomy was made under isoflurane anesthesia and an atraumatic vascular

306 clamp placed on the portal vein and the hepatic artery to block blood flow to the left and medial
307 lobes of the liver which account for about 70% of the liver parenchyma. The clamp was removed
308 after 1 h to allow for reperfusion. Following 6 h of reperfusion, mice were euthanized before
309 blood and tissue collection for analysis.
310
311 *Reagents*
312 Mammalian expression vectors were obtained from the following sources: 2xSidM-GFP
313 as described in (Levin et al. 2017); EGFP-Vimentin-7 was a gift from Michael Davidson
314 (Addgene plasmid # 56439); pCAG mEmerald-LAMP1 was a gift from Franck Polleux (Addgene
315 plasmid # 168513). Human NLRP3 from pEGFP-C2-NLRP3 (gift from Christian Stehlik
316 (Addgene plasmid # 73955)) was inserted into an mCherry-C2 mammalian vector by Gibson
317 assembly cloning (NEB, cat #E2611S); 2xFyve-GFP as described in (Gillooly 2000); and
318 pJSK659 (SNx-A-GFP) was a gift from Jason King (Addgene plasmid # 205128). Primary
319 antibodies used were: rabbit anti-cleaved caspase-1 (Asp296) (E2G2I) (Cell Signaling, cat
320 #89332), mouse anti-ASC (BioLegend, cat #676502), rabbit anti-vimentin (Cell Signaling, cat
321 #5741), rabbit anti-pro caspase-1 + p10 +p12 (Abcam, cat. #ab179515) and rabbit anti-GAPDH
322 (Cell Signalling, cat #2118S). Secondary antibodies conjugated with AlexaFluor-405, -488, -555,
323 -647 and donkey anti-goat HRP secondary antibodies were obtained from Jackson
324 ImmunoResearch. Secondary mouse and rabbit antibodies conjugated with HRP were obtained
325 from Cell Signaling.
326 Cell culture reagents used include Dulbecco's modified eagle medium (DMEM, Wisent,
327 cat. #319-007-CL), fetal bovine serum (Atlanta Biologicals, cat. #S12450), Gibco™ DMEM, high
328 glucose, HEPES, no phenol red (FischerScientific, cat. #21063029), HBSS w/out phenol red,
329 calcium and magnesium, supplemented with FBS (Wisent, cat. #311-512 CL**),** 100x antibiotic-
330 antimycotic solution (Wisent, cat. #450-115-CL), FuGENE 6 Transfection reagent (Promega,
331 cat. #E2691), phosphate buffered saline (Wisent, Sigma-Aldrich, cat#311-010-CL), nigericin

332 sodium salt (Cayman chemicals, cat. #11437), adenosine triphosphate (pH=7.4, cat. #A2383-
333 5G), propidium iodide (Invitrogen, cat. #P1304MP), alum hydroxide (Invivogen, cat. #21645-51-
334 2), monosodium urate crystals (Invivogen, cat. #1198-77-2), lipopolysaccharide (Sigma-Aldrich,
335 cat. # L9764-5MG), concanamycin A (Cayman, cat. # 11050), Prolong Gold Mounting medium
336 with DAPI (Invitrogen, cat #P36935). .
337
338 *Cell culture*
339 Bone marrow derived macrophages from the long bones of 6-12-wk-old wt and *Vim*$^{-/-}$
340 mice was harvested by centrifugation and grown in DMEM + 10% FBS + 10% macrophage
341 colony stimulating factor (MCSF) + 1% penicillin-streptomycin at 37°C and under 5% CO_2. Cells
342 were used 5-7 days after isolation. HeLa cells were grown and passaged in DMEM + 5% FBS +
343 1% penicillin-streptomycin at 37°C and under 5% CO_2.
344
345 *Transfections*
346 HeLa cells were seeded on top of coverslips in 12-well plates and left to attach overnight
347 at 37°C and under 5% CO_2. FuGENE6 Transfection reagent was added to room temperature
348 serum-free DMEM for 5 min, and then plasmid DNA was added at a 1:3 ratio of DNA (μg) to
349 FuGENE6 (μL). Mixture was incubated at room temperature for 15 min and added to each well.
350 Cells were transfected at ~60% confluency and incubated for at least 18 h at 37°C and under
351 5% CO_2 after transfection.
352
353 *Intracellular [K^+] measurements*
354 BMDM were grown to 90% confluency in 2 separate 6-well plates with DMEM
355 supplemented with 10% FBS and 10% MCSF. Following nigericin or ATP stimulation, BMDM
356 from one plate were washed 3x in 150 mM LiCl (pH=7.4) and lysed in 5 mM HNO_3. Cell lysates

357 were incubated at 4°C overnight and centrifuged at 12,000 g for 15 min to remove any debris.
358 Samples and standards of known [K^+] were analyzed using a PinAAcle 900T Atomic Absorption
359 Spectrometer (PerkinElmer, Waltham, MA, USA) to assess the total amount of K^+ ions. In
360 parallel, BMDM from the second plate were washed as previously described and lifted in
361 isotonic solution. Cell concentration and volumes were determined electronically using a Z2
362 Coulter particle count and size analyzer (Beckman Coulter) to calculate total cell number and
363 volume for each sample. Intracellular concentrations of K+ were calculated by dividing the total
364 ion content by the total cell volume of each well.
365
366 *Immunostaining*
367 BMDM were grown to 70-80% confluency in 12-well plates with DMEM supplemented
368 with 10% FBS and 10% MCSF. Then, BMDM were primed with LPS (1 μg/mL, 4h) and
369 subsequently treated with nigericin (10 μM, 30 min) or ATP (3 mM, 1h). Cells were then fixed
370 with 4% PFA for 15 min, permeabilized in 0.1% triton for 5 min and blocked in 5% BSA
371 overnight. Primary and secondary antibodies were diluted to 1:100 and 1:500 in 2.5% BSA in
372 PBS, respectively, and added to coverslips at room temperature for 1 h. Coverslips were
373 washed 3 times with PBS following incubation. Slides were mounted using mounting media
374 containing DAPI.
375
376 *PI assay*
377 BMDM were grown to 70-80% confluency in 12 well plates with DMEM supplemented
378 with 10% FBS and 10% MCSF. Cells were primed with LPS (1 μg/mL) for 4 h before
379 simultaneously adding nigericin (10 μM) and 0.3 μg/mL of propidium iodide. Pictures of each
380 well were taken every 15 min in both brightfield and RFP setting of an EVOS microscope

381 (ThermoFischer). At least 3 images of different fields of view were obtained per well per
382 timepoint.
383
384 *LDH assay*
385 Cells were grown to 80-90% confluency in 12 well plates with DMEM supplemented with
386 10% FBS and 10% MCSF. Priming with LPS (1 μg/mL) was done for 4 h, then cells were treated
387 with nigericin (10 μM) for 30 min, ATP (3 mM) for 1 h, alum (100 μg/ml) for 6 h, or MSU (100
388 μg/ml) for 16 h in 0.1% FBS DMEM. The supernatants of each well were collected and
389 centrifuged at 13,000 g for 5 min, and cells in each well were washed with 1x PBS and lysed in
390 RIPA buffer with protease inhibitor. LDH release was assayed according to manual instructions
391 of the LDH assay kit (CyQUANT LDH Cytotoxicity Assay, Invitrogen, cat #C20301).
392
393 *Western blotting*
394 BMDM were grown to 80-90% confluency in 6 well plates with 10% FBS and 10%
395 MCSF. Cells were primed with LPS (1 μg/mL) for 4 h, then treated in reduced serum medium
396 (0.1% FBS) with either nigericin (10 μM) for 30 min or ATP (3 mM) for 1 h. Supernatants were
397 prepared following the TCA precipitation protocol from (Volchuk et al. 2020). Briefly, samples
398 were centrifuged at 13,000 g for 5 min at 4°C to remove any debris and precipitated using 100%
399 TCA. Samples were then washed with ice cold acetone, then heated at 95° C, and finally
400 resuspended in 2x SDS-PAGE sample buffer. For the cell lysates, cells were washed with 1x D-
401 PBS and lysed with RIPA buffer with protease inhibitors. Lysates were centrifuged at 12,000 g
402 for 15 min at 4°C and prepared after determining protein concentration by BCA assay. Lysate
403 proteins were resolved in a 12% SDS-PAGE gel and supernatant proteins using a 15% SDS-
404 PAGE gel. Proteins were transferred to a PVDF membrane and immunoblotted with the

405 appropriate antibodies. Images were analyzed using ImageJ to determine the adjusted mean
406 gray intensity value of each band over the same area.
407
408 *IL-1β Enzyme linked immunosorbent assay (ELISA)*
409 BMDM were grown on 24-well plates to 80-90% confluency using DMEM supplemented
410 with 10% FBS and 10% MCSF. BMDM were stimulated as previously described and
411 supernatants were collected and centrifuged for 5 min (10,000 rpm, 4°C). ELISAs were
412 performed according to the manufacturer's instructions (Mouse IL-1 beta ELISA kit, Abcam, cat.
413 #ab100705). Sample absorbance was read using a Varioskan LUX Plate Reader 1 w/Dual
414 Injectors (Thermofischer Scientific)
415
416 *Microscopy*
417 Cells immunostained for ASC and vimentin were visualized by confocal microscopy
418 using a spinning-disk Zeiss Axiovert 200 M microscope (Quorum Technologies Inc.) with an
419 ORCA-Fusion BT cMOS camera, a five-line laser module with 405-, 443-, 491-, 561-, and 655-
420 nm lines. The microscope operating software was Volocity v6.3 (Perkin Elmer). Images were
421 acquired as Z-stacks with a 63×/1.4 NA for Vimentin/ASC images and 25x/0.8 NA water
422 objective for ASC-speck quantification images.
423 Live confocal fluorescence imaging of mCherry-NLRP3, LAMP1-mEmerald, and
424 phosphoinositide probes was done using a Zeiss Axio Observer microscope with a PCO camera
425 and four-line laser module with 405-, 443-, 491-, and 561-nm lines. Coverslips with cells were
426 placed in a chamber with HBSS and imaged on a pre-warmed stage and 63×/1.4 NA oil
427 objective to 37° C. Coverslips used to acquire movies were placed in a chamber along with
428 phenol red-free DMEM and an environmental control chamber set to 37° C and 5% CO_2. Movies
429 were acquired as single-slice images over the course of one hour.

Image analysis

Liver tissue was fixed in PFA and stained with hematoxylin and eosin. Slides were digitalized and ischemic score was determined using the DenseNetV2 identifier available in the HALO software. ASC-speck positivity and Pearson's correlation analysis were done using the Volocity software over the ROI of individual cells. Pearson's correlation image thresholding was done according to the (Costes et al. 2004) thresholding method to avoid any bias. PI positivity analysis was done in ImageJ using the "Cell counter" feature to obtain the total number of PI positive cells per field of view and the total number of cells per field of view.

SODA analysis of HeLa cells expressing mCherry-NLRP3 and the phosphoinositide probes was done using the free image analysis software called Icy (http://icy.bioimageanalysis.org/) and using a modified protocol from (Lagache et al. 2018). Briefly, detection of bright spots on single slice two-channel images was calibrated using the Wavelet Spot Detector. Then, ROIs were made for each individual cell and the statistical probability that spots from both channels were associated with each other by random chance was calculated (as defined by $p > 0.05$). Probability was found for different radii (*r)* distances from the centre of each spot. Represented in our figure is the coupled puncta of NLRP3 within $r = 6$ pixels (~516 nm).

Data analysis

Statistical significance for *in vitro* experiments was determined using a two-way ANOVA with Tukey's multiple comparisons test (significant difference threshold $P < 0.05$). For *in* vivo experiments, an unpaired Student's *t* tests (significant difference threshold $P < 0.05$) was used. All non-surgical and surgical experimental data is presented as the mean ± SEM or SD. All data analysis was done using GraphPad Prism 6 and Excel.

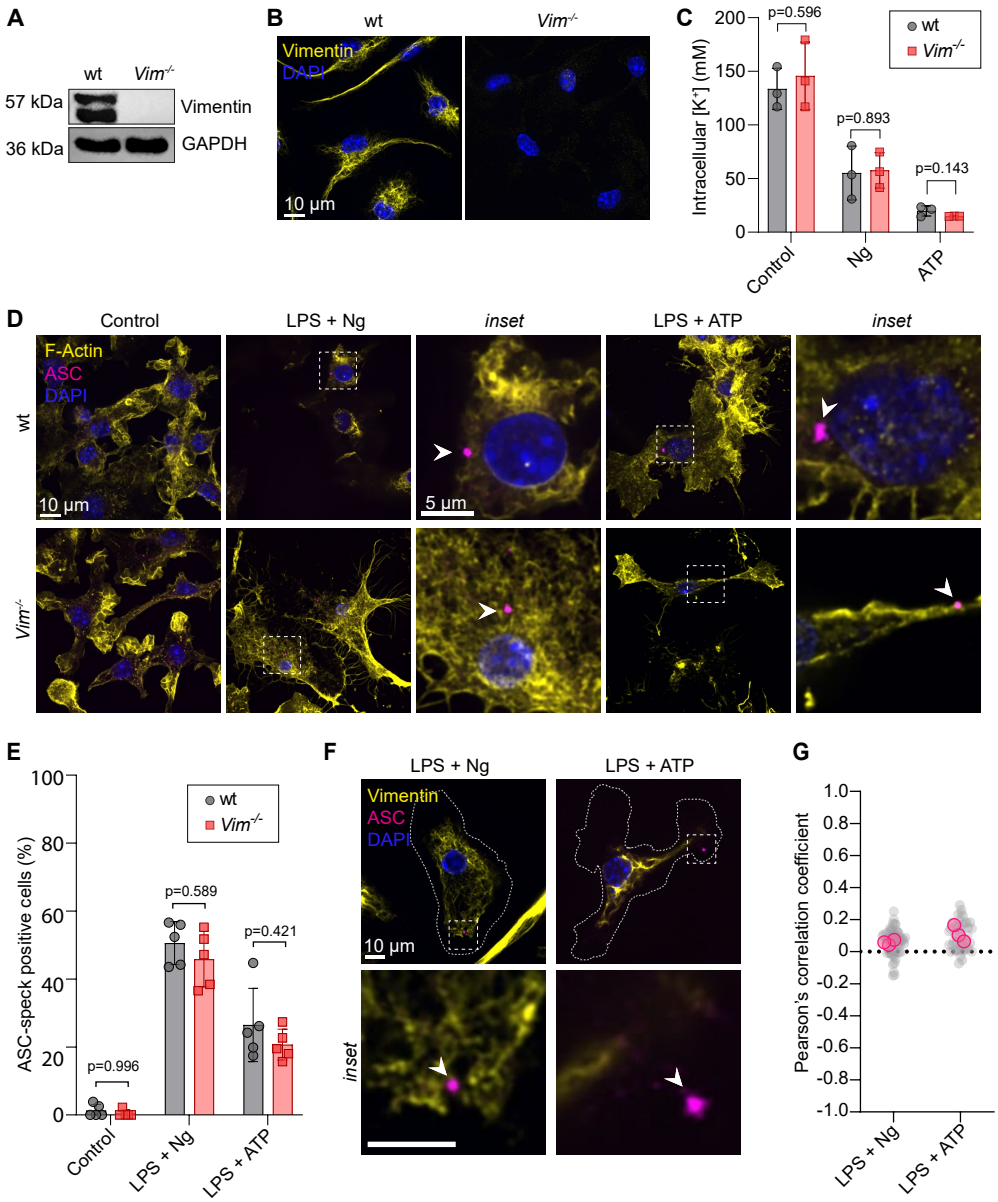

Figure 1. K^+-dependent ASC aggregation remains unaffected by the absence of vimentin intermediate filaments. Validation of *Vim*$^{-/-}$ BMDM by **(A)** western blot and **(B)** vimentin immunostaining as compared to wt control BMDM. **(C)** Intracellular BMDM concentrations of K^+ were measured by atomic absorption spectrometry in BMDM derived from C57/Bl6 mice following treatment with nigericin for 15 min or ATP for 30 min. Replicate mean ± SD are shown (N=3) **(D, E, F, G)** wt and *Vim*$^{-/-}$ BMDM were primed with LPS (1 µg/mL, 4 h) and treated with nigericin (10 µM, 30 min) or ATP (3 mM, 1 h) and imaged using a confocal microscope. **(D,E)** Formation of "ASC-specks" was visualized by immunostaining of wt and Vim$^{-/-}$ BMDM, along with F-actin (phalloidin) and DAPI counterstaining. Representative image shown in **D.** Data are shown as mean of each replicate ± SEM in **E** (N=5). **(F,G)** Co-localization of vimentin and "ASC-specks" was visualized by immunostaining of vimentin and ASC in BMDM derived from C57/Bl6 mice. Representative image shown in **F.** Pearson's correlation coefficient mean (minimum 7 cells per replicate) ± SD data are shown in **G** (N=3). Scale bar 10 µm, insets 5 µm.

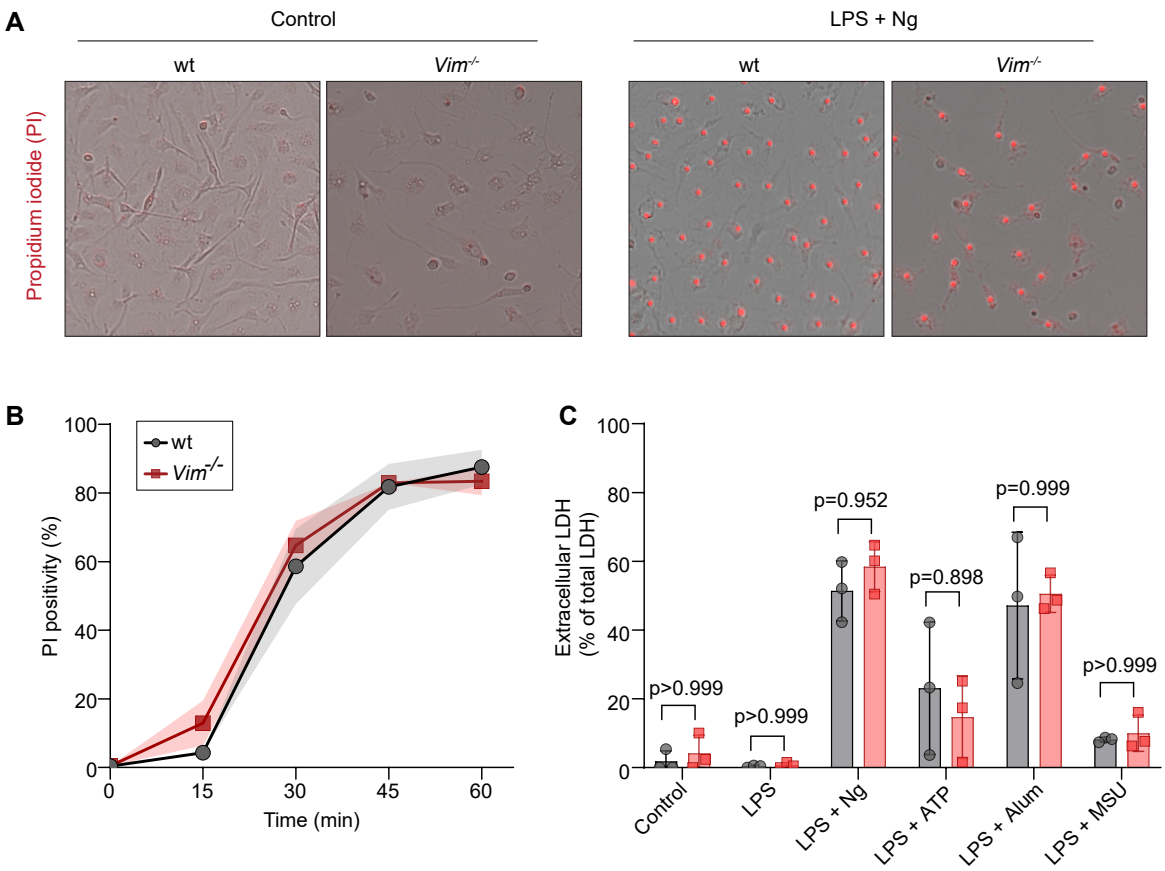

Figure 2. Pyroptotic cell death downstream on NLRP3 inflammasome activation is not dependent on vimentin intermediate filaments. (A,B) wt and *Vim*$^{-/-}$ BMDM were primed with LPS (1 μg/mL, 4 h) before the addition of propidium iodide (1 μg/mL) along with nigericin (10 μM). **(Fig. 2A,B)**. Percent PI positivity is displayed in **B** as the mean ± SEM of each timepoint. (N=3) **(C)** Release of LDH was determined in wt and *Vim*$^{-/-}$ BMDM that were primed with LPS (1 μg/mL, 4 h) and treated with nigericin (10 μM) for 30 min, ATP (3 mM) for 1 h, alum (100 μg/ml) for 6 h, or MSU (100 μg/ml) for 16 h. Data represented as mean ± SD (N=3)

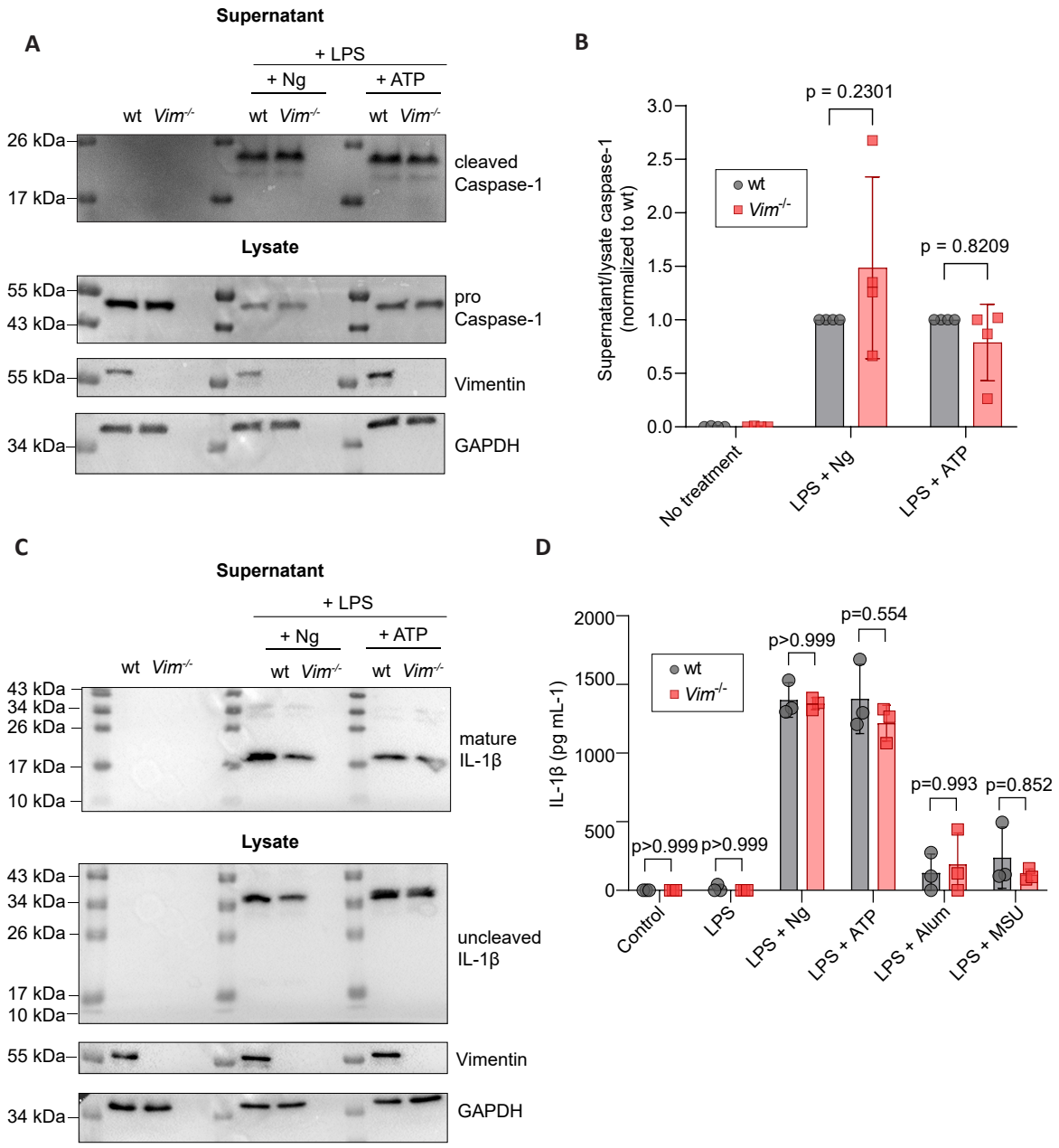

Figure 3. *Vim*$^{-/-}$ BMDM cleave and release caspase-1 and IL-1β following NLRP3 inflammasome activation. BMDM were primed with LPS (1 μg/mL, 4 h) and treated with nigericin (10 μM, 30 min) or ATP (3 mM, 1 h). Samples were visualized by SDS-PAGE. **(A)** Western blots of cell lysates and supernatants against uncleaved and cleaved capase-1, respectively. **(B)** Quantification of ratio of cleaved to uncleaved caspase-1 normalized to wt treatments. **(C)** Western blots of cell lysates and supernatants against immature and mature IL-1β, respectively. **(D)** Levels of extracellular IL-1β in LPS-primed wt and *Vim*$^{-/-}$ BMDM treated with nigericin and ATP as previously described, along with alum (100 μg/ml, 6 h) or MSU (100 μg/ml, 16 h) treatments. Mature IL-1β concentration from cell supernatants was measured by ELISA. Data represented as replicate means ± SD (minimum N=3).

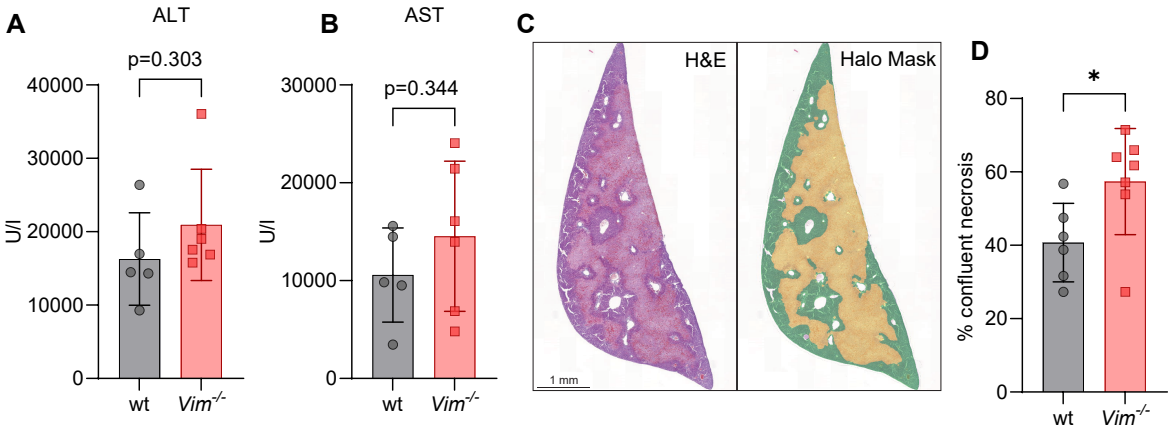

Figure 4. *Vim*$^{-/-}$ mice are not ostensibly protected against hepatic ischemia/reperfusion injury. Warm ischemia/reperfusion injury was modeled using male wt (C57Bl/6) control and *Vim*$^{-/-}$ mice between 6-12 weeks of age. **(A,B)** Levels of aspartate aminotransferase (AST) and alanine aminotransferase (ALT) in the serum of mice were measured. **(C)** Hematoxylin and eosin (H&E) staining of liver tissue samples along with Halo DenseNetV2 mask to detect healthy and necrotic areas. **(D)** Quantification of percent necrosis of liver samples. Data shown as biological replicates ± SD (wt N=7, Vim$^{-/-}$ N=6 mice per group.) (*$p < 0.05$)

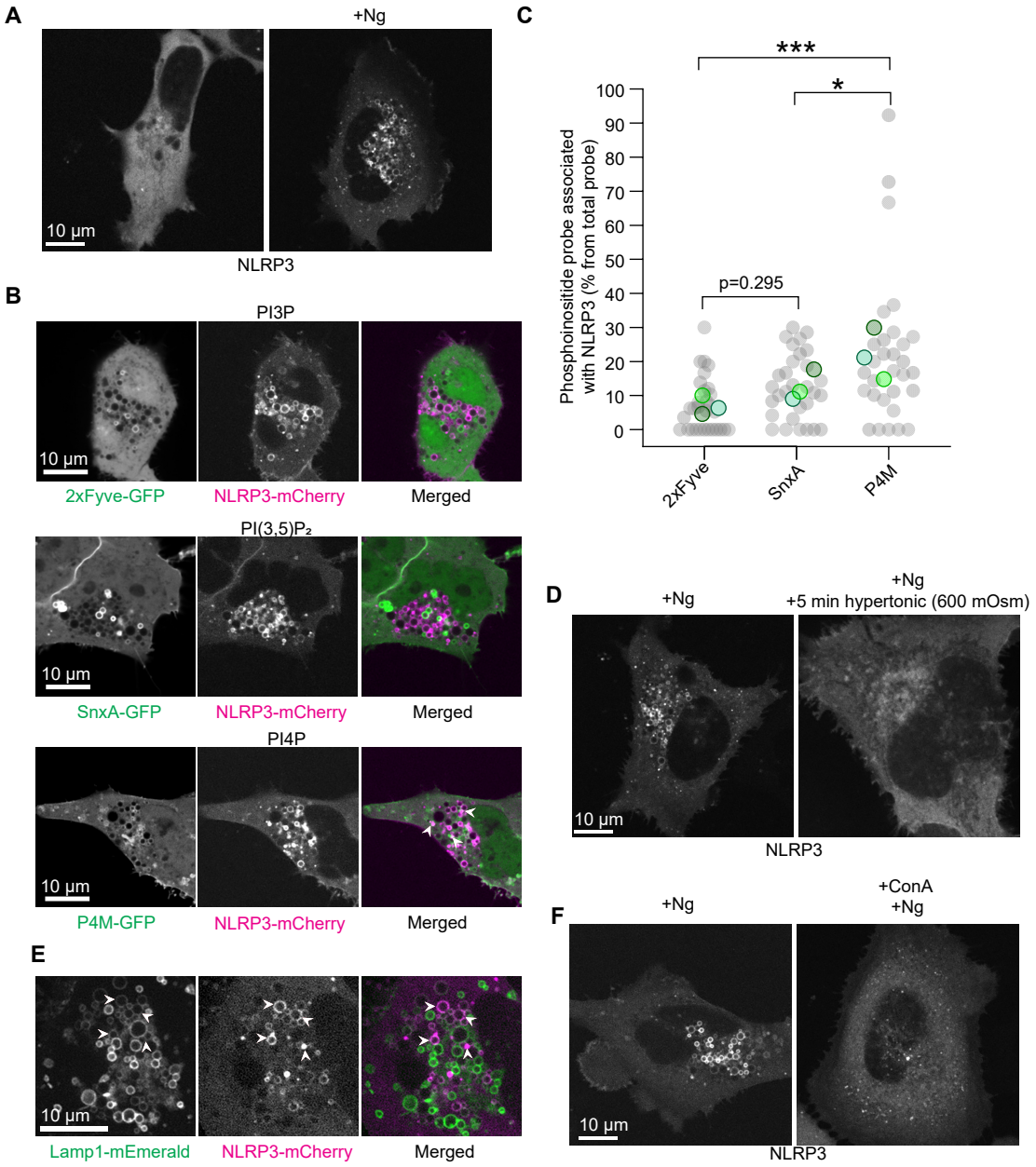

Figure 5. NLRP3 aggregates on swollen, PI4P- and LAMP1-positive vesicular compartments. (A) HeLa cells expressing mCherry-NLRP3 before and after treatment with nigericin (10 µM, 1h). **(B)** Co-expression of mCherry-NLRP3 with 2xFyve-GFP, SnxA-GFP, or P4M-GFP phosphoinositide probes following nigericin treatment (10 µM, 1h). Images shown as slices from Z-stack projection. **(C)** SODA analysis for object association. Data represented as distribution of percent NLRP3 objects coupled with phosphoinositide probe objects. (N=3, with 10 cells per technical replicate, *p<0.05, ***p<0.0005). **(D)** HeLa cells expressing mCherry-NLRP3 treated with nigericin for 1 h prior to hypertonic shock. Medium osmolarity was increased using 1M sucrose for 5 min. **(E)** Nigericin-treated HeLa cells expressing mCherry-NLRP3 with LAMP1-GFP. **(F)** HeLa cells expressing mCherry-NLRP3 treated with nigericin with or without pre-treatment with concanamycin A (1 µM, 30 min). Scale bar, 10 µm.

References

Barberis, Laura, Christian Pasquali, Dominique Bertschy-Meier, Alessandra Cuccurullo, Carlotta Costa, Chiara Ambrogio, Francis Vilbois, et al. 2009. “Leukocyte Transmigration Is Modulated by Chemokine-Mediated PI3Kγ-Dependent Phosphorylation of Vimentin.” *European Journal of Immunology* 39 (4): 1136–46. https://doi.org/10.1002/eji.200838884.

Battaglia, Rachel A., Samed Delic, Harald Herrmann, and Natasha T. Snider. 2018. “Vimentin on the Move: New Developments in Cell Migration.” *F1000Research* 7 (November):1796. https://doi.org/10.12688/f1000research.15967.1.

Bauernfeind, Franz G., Gabor Horvath, Andrea Stutz, Emad S. Alnemri, Kelly MacDonald, David Speert, Teresa Fernandes-Alnemri, et al. 2009. “Cutting Edge: NF-κB Activating Pattern Recognition and Cytokine Receptors License NLRP3 Inflammasome Activation by Regulating NLRP3 Expression.” *The Journal of Immunology* 183 (2): 787–91. https://doi.org/10.4049/jimmunol.0901363.

Brough, David, and Nancy J. Rothwell. 2007. “Caspase-1-Dependent Processing of pro-Interleukin-1β Is Cytosolic and Precedes Cell Death.” *Journal of Cell Science* 120 (5): 772–81. https://doi.org/10.1242/jcs.03377.

Chen, Jueqi, and Zhijian J. Chen. 2018. “PtdIns4P on Dispersed Trans-Golgi Network Mediates NLRP3 Inflammasome Activation.” *Nature* 564 (7734): 71–76. https://doi.org/10.1038/s41586-018-0761-3.

Colucci-Guyon, Emma, Marie-Madeleine Portier, Irene Dunia, Denise Paulin, Sandrine Pournin, and Charles Babinet. 1994. “Mice Lacking Vimentin Develop and Reproduce without an Obvious Phenotype.” *Cell* 79 (4): 679–94. https://doi.org/10.1016/0092-8674(94)90553-3.

Compan, Vincent, Alberto Baroja-Mazo, Gloria López-Castejón, Ana I. Gomez, Carlos M. Martínez, Diego Angosto, María T. Montero, et al. 2012. “Cell Volume Regulation Modulates NLRP3 Inflammasome Activation.” *Immunity* 37 (3): 487–500. https://doi.org/10.1016/j.immuni.2012.06.013.

Costes, Sylvain V., Dirk Daelemans, Edward H. Cho, Zachary Dobbin, George Pavlakis, and Stephen Lockett. 2004. “Automatic and Quantitative Measurement of Protein-Protein Colocalization in Live Cells.” *Biophysical Journal* 86 (6): 3993–4003. https://doi.org/10.1529/biophysj.103.038422.

Eckes, B., E. Colucci-Guyon, H. Smola, S. Nodder, C. Babinet, T. Krieg, and P. Martin. 2000. “Impaired Wound Healing in Embryonic and Adult Mice Lacking Vimentin.” *Journal of Cell Science* 113 (13): 2455–62. https://doi.org/10.1242/jcs.113.13.2455.

Evavold, Charles L., Jianbin Ruan, Yunhao Tan, Shiyu Xia, Hao Wu, and Jonathan C. Kagan. 2018. “The Pore-Forming Protein Gasdermin D Regulates Interleukin-1 Secretion from Living Macrophages.” *Immunity* 48 (1): 35-44.e6. https://doi.org/10.1016/j.immuni.2017.11.013.

Fang, Run, Qifei Jiang, Xinying Jia, and Zhengfan Jiang. 2023. “ARMH3-Mediated Recruitment of PI4KB Directs Golgi-to-Endosome Trafficking and Activation of the Antiviral Effector STING.” *Immunity* 56 (3): 500-515.e6. https://doi.org/10.1016/j.immuni.2023.02.004.

Fink, Susan L., and Brad T. Cookson. 2006. “Caspase-1-Dependent Pore Formation during Pyroptosis Leads to Osmotic Lysis of Infected Host Macrophages.” *Cellular Microbiology* 8 (11): 1812–25. https://doi.org/10.1111/j.1462-5822.2006.00751.x.

Franchi, Luigi, and Gabriel Núñez. 2008. “The Nlrp3 Inflammasome Is Critical for Aluminium Hydroxide-Mediated IL-1β Secretion but Dispensable for Adjuvant Activity.” *European Journal of Immunology* 38 (8): 2085–89. https://doi.org/10.1002/eji.200838549.

Gillooly, D. J. 2000. “Localization of Phosphatidylinositol 3-Phosphate in Yeast and Mammalian Cells.” *The EMBO Journal* 19 (17): 4577–88. https://doi.org/10.1093/emboj/19.17.4577.

Greaney, Allison J., Stephen H. Leppla, and Mahtab Moayeri. 2015. “Bacterial Exotoxins and the Inflammasome.” *Frontiers in Immunology* 6 (November). https://doi.org/10.3389/fimmu.2015.00570.

Groß, Christina J., Ritu Mishra, Katharina S. Schneider, Guillaume Médard, Jennifer Wettmarshausen, Daniela C. Dittlein, Hexin Shi, et al. 2016. “K + Efflux-Independent NLRP3 Inflammasome Activation by Small Molecules Targeting Mitochondria.” *Immunity* 45 (4): 761–73. https://doi.org/10.1016/j.immuni.2016.08.010.

Hari, Aswin, Yifei Zhang, Zhongyuan Tu, Pascal Detampel, Melanie Stenner, Anutosh Ganguly, and Yan Shi. 2014. “Activation of NLRP3 Inflammasome by Crystalline Structures via Cell Surface Contact.” *Scientific Reports* 4 (1): 7281. https://doi.org/10.1038/srep07281.

Håversen, Liliana, Jeanna Perman Sundelin, Adil Mardinoglu, Mikael Rutberg, Marcus Ståhlman, Ulrika Wilhelmsson, Lillemor Mattsson Hultén, et al. 2018. “Vimentin Deficiency in Macrophages Induces Increased Oxidative Stress and Vascular Inflammation but Attenuates Atherosclerosis in Mice.” *Scientific Reports* 8 (1): 16973. https://doi.org/10.1038/s41598-018-34659-2.

He, Wan-ting, Haoqiang Wan, Lichen Hu, Pengda Chen, Xin Wang, Zhe Huang, Zhang-Hua Yang, Chuan-Qi Zhong, and Jiahuai Han. 2015. “Gasdermin D Is an Executor of Pyroptosis and Required for Interleukin-1β Secretion.” *Cell Research* 25 (12): 1285–98. https://doi.org/10.1038/cr.2015.139.

Hornung, Veit, Franz Bauernfeind, Annett Halle, Eivind O Samstad, Hajime Kono, Kenneth L Rock, Katherine A Fitzgerald, and Eicke Latz. 2008. “Silica Crystals and Aluminum Salts Activate the NALP3 Inflammasome through Phagosomal Destabilization.” *Nature Immunology* 9 (8): 847–56. https://doi.org/10.1038/ni.1631.

Ivaska, Johanna, Hanna-Mari Pallari, Jonna Nevo, and John E. Eriksson. 2007. “Novel Functions of Vimentin in Cell Adhesion, Migration, and Signaling.” *Experimental Cell Research* 313 (10): 2050–62. https://doi.org/10.1016/j.yexcr.2007.03.040.

Jaeschke, Hartmut. 2003. “Molecular Mechanisms of Hepatic Ischemia-Reperfusion Injury and Preconditioning.” *American Journal of Physiology-Gastrointestinal and Liver Physiology* 284 (1): G15–26. https://doi.org/10.1152/ajpgi.00342.2002.

Jiang, Susan X., Jacqueline Slinn, Amy Aylsworth, and Sheng T. Hou. 2012. “Vimentin Participates in Microglia Activation and Neurotoxicity in Cerebral Ischemia: Vimentin Controls Microglia Activation.” *Journal of Neurochemistry* 122 (4): 764–74. https://doi.org/10.1111/j.1471-4159.2012.07823.x.

Jiménez-Castro, Mónica B., María Eugenia Cornide-Petronio, Jordi Gracia-Sancho, and Carmen Peralta. 2019. “Inflammasome-Mediated Inflammation in Liver Ischemia-Reperfusion Injury.” *Cells* 8 (10): 1131. https://doi.org/10.3390/cells8101131.

Kelley, Nathan, Devon Jeltema, Yanhui Duan, and Yuan He. 2019. “The NLRP3 Inflammasome: An Overview of Mechanisms of Activation and Regulation.” *International Journal of Molecular Sciences* 20 (13): 3328. https://doi.org/10.3390/ijms20133328.

599 Lagache, Thibault, Alexandre Grassart, Stéphane Dallongeville, Orestis Faklaris, Nathalie
600 Sauvonnet, Alexandre Dufour, Lydia Danglot, and Jean-Christophe Olivo-Marin. 2018.
601 "Mapping Molecular Assemblies with Fluorescence Microscopy and Object-Based Spatial
602 Statistics." *Nature Communications* 9 (1): 698. https://doi.org/10.1038/s41467-018-
603 03053-x.
604 Laliberte, Ronald E., James Eggler, and Christopher A. Gabel. 1999. "ATP Treatment of Human
605 Monocytes Promotes Caspase-1 Maturation and Externalization." *Journal of Biological*
606 *Chemistry* 274 (52): 36944–51. https://doi.org/10.1074/jbc.274.52.36944.
607 Li, Hanfen, Stephen B. Willingham, Jenny P.-Y. Ting, and Fabio Re. 2008. "Cutting Edge:
608 Inflammasome Activation by Alum and Alum's Adjuvant Effect Are Mediated by NLRP3."
609 *Journal of Immunology (Baltimore, Md.: 1950)* 181 (1): 17–21.
610 https://doi.org/10.4049/jimmunol.181.1.17.
611 Li, Hao, Yanling Guan, Bo Liang, Peng Ding, Xin Hou, Wei Wei, and Yang Ma. 2022. "Therapeutic
612 Potential of MCC950, a Specific Inhibitor of NLRP3 Inflammasome." *European Journal of*
613 *Pharmacology* 928 (August):175091. https://doi.org/10.1016/j.ejphar.2022.175091.
614 Li, Jichang, Jie Zhao, Min Xu, Meng Li, Bingrui Wang, Xiaoye Qu, Chang Yu, et al. 2020. "Blocking
615 GSDMD Processing in Innate Immune Cells but Not in Hepatocytes Protects Hepatic
616 Ischemia–Reperfusion Injury." *Cell Death & Disease* 11 (4): 244.
617 https://doi.org/10.1038/s41419-020-2437-9.
618 Luteijn, Rutger D., Sypke R. Van Terwisga, Jill E. Ver Eecke, Liberty Onia, Shivam A. Zaver, Joshua
619 J. Woodward, Richard W. Wubbolts, David H. Raulet, and Frank J. M. Van Kuppeveld.
620 2024. "The Activation of the Adaptor Protein STING Depends on Its Interactions with the
621 Phospholipid PI4P." *Science Signaling* 17 (827): eade3643.
622 https://doi.org/10.1126/scisignal.ade3643.
623 Man, Si Ming, Lee J. Hopkins, Eileen Nugent, Susan Cox, Ivo M. Glück, Panagiotis Tourlomousis,
624 John A. Wright, Pietro Cicuta, Tom P. Monie, and Clare E. Bryant. 2014. "Inflammasome
625 Activation Causes Dual Recruitment of NLRC4 and NLRP3 to the Same Macromolecular
626 Complex." *Proceedings of the National Academy of Sciences* 111 (20): 7403–8.
627 https://doi.org/10.1073/pnas.1402911111.
628 Mangan, Matthew S.J., Anil Akbal, Sophie Rivara, Agnes Schröder, Gabor Horvath, Philipp Walch,
629 Jan Hegermann, et al. 2024. "Cytosolic Sodium Accumulation Is a Common Danger Signal
630 Triggering Endocytic Dysfunction and NLRP3 Inflammasome Activation."
631 https://doi.org/10.1101/2024.03.26.586774.
632 Martinon, Fabio, Virginie Pétrilli, Annick Mayor, Aubry Tardivel, and Jürg Tschopp. 2006. "Gout-
633 Associated Uric Acid Crystals Activate the NALP3 Inflammasome." *Nature* 440 (7081):
634 237–41. https://doi.org/10.1038/nature04516.
635 Mayes-Hopfinger, Lindsey, Aura Enache, Jian Xie, Chou-Long Huang, Robert Köchl, Victor L. J.
636 Tybulewicz, Teresa Fernandes-Alnemri, and Emad S. Alnemri. 2021. "Chloride Sensing by
637 WNK1 Regulates NLRP3 Inflammasome Activation and Pyroptosis." *Nature*
638 *Communications* 12 (1): 4546. https://doi.org/10.1038/s41467-021-24784-4.
639 Mor-Vaknin, Nirit, Maureen Legendre, Yue Yu, Carlos H. C. Serezani, Sanjay K. Garg, Anna Jatzek,
640 Michael D. Swanson, et al. 2013. "Murine Colitis Is Mediated by Vimentin." *Scientific*
641 *Reports* 3 (1): 1045. https://doi.org/10.1038/srep01045.

642 Muñoz-Planillo, Raúl, Peter Kuffa, Giovanny Martínez-Colón, Brenna L. Smith, Thekkelnaycke M.
643 Rajendiran, and Gabriel Núñez. 2013. "K+ Efflux Is the Common Trigger of NLRP3
644 Inflammasome Activation by Bacterial Toxins and Particulate Matter." *Immunity* 38 (6):
645 1142–53. https://doi.org/10.1016/j.immuni.2013.05.016.
646 Nieminen, Mikko, Tiina Henttinen, Marika Merinen, Fumiko Marttila–Ichihara, John E. Eriksson,
647 and Sirpa Jalkanen. 2006. "Vimentin Function in Lymphocyte Adhesion and Transcellular
648 Migration." *Nature Cell Biology* 8 (2): 156–62. https://doi.org/10.1038/ncb1355.
649 Pelegrin, Pablo, and Annmarie Surprenant. 2006. "Pannexin-1 Mediates Large Pore Formation
650 and Interleukin-1β Release by the ATP-Gated P2X7 Receptor." *The EMBO Journal* 25 (21):
651 5071–82. https://doi.org/10.1038/sj.emboj.7601378.
652 Perregaux, D., and C. A. Gabel. 1994. "Interleukin-1 Beta Maturation and Release in Response to
653 ATP and Nigericin. Evidence That Potassium Depletion Mediated by These Agents Is a
654 Necessary and Common Feature of Their Activity." *The Journal of Biological Chemistry*
655 269 (21): 15195–203.
656 Santos, Gimena dos, Micah R. Rogel, Margaret A. Baker, James R. Troken, Daniela Urich, Luisa
657 Morales-Nebreda, Joseph A. Sennello, et al. 2015. "Vimentin Regulates Activation of the
658 NLRP3 Inflammasome." *Nature Communications* 6 (1): 6574.
659 https://doi.org/10.1038/ncomms7574.
660 Schmacke, Niklas A., Fionan O'Duill, Moritz M. Gaidt, Inga Szymanska, Julia M. Kamper,
661 Jonathan L. Schmid-Burgk, Sophia C. Mädler, et al. 2022. "IKKβ Primes Inflammasome
662 Formation by Recruiting NLRP3 to the Trans-Golgi Network." *Immunity* 55 (12): 2271-
663 2284.e7. https://doi.org/10.1016/j.immuni.2022.10.021.
664 Schorn, Christine, Benjamin Frey, Kirsten Lauber, Christina Janko, Moritz Strysio, Hildegard
665 Keppeler, Udo S. Gaipl, et al. 2011. "Sodium Overload and Water Influx Activate the
666 NALP3 Inflammasome." *Journal of Biological Chemistry* 286 (1): 35–41.
667 https://doi.org/10.1074/jbc.M110.139048.
668 Selzner, Nazia, Markus Selzner, Wolfram Jochum, and Pierre-Alain Clavien. 2003. "Ischemic
669 Preconditioning Protects the Steatotic Mouse Liver against Reperfusion Injury: An ATP
670 Dependent Mechanism." *Journal of Hepatology* 39 (1): 55–61.
671 https://doi.org/10.1016/S0168-8278(03)00147-8.
672 Tan, Julie, and Julie A. Brill. 2014. "Cinderella Story: PI4P Goes from Precursor to Key Signaling
673 Molecule." *Critical Reviews in Biochemistry and Molecular Biology* 49 (1): 33–58.
674 https://doi.org/10.3109/10409238.2013.853024.
675 Vines, James H., Hannes Maib, Catherine M. Buckley, Aurelie Gueho, Zhou Zhu, Thierry Soldati,
676 David H. Murray, and Jason S. King. 2023. "A PI(3,5)P2 Reporter Reveals PIKfyve Activity
677 and Dynamics on Macropinosomes and Phagosomes." *Journal of Cell Biology* 222 (9):
678 e202209077. https://doi.org/10.1083/jcb.202209077.
679 Volchuk, Allen, Anna Ye, Leon Chi, Benjamin E. Steinberg, and Neil M. Goldenberg. 2020.
680 "Indirect Regulation of HMGB1 Release by Gasdermin D." *Nature Communications* 11
681 (1): 4561. https://doi.org/10.1038/s41467-020-18443-3.
682 Wu, Tong, Cheng Zhang, Tianfeng Shao, Jianzhong Chen, and Diyu Chen. 2022. "The Role of
683 NLRP3 Inflammasome Activation Pathway of Hepatic Macrophages in Liver Ischemia–
684 Reperfusion Injury." *Frontiers in Immunology* 13 (June):905423.
685 https://doi.org/10.3389/fimmu.2022.905423.

686 Yu, Shi, Jack Green, Rose Wellens, Gloria Lopez-Castejon, and David Brough. 2021. "Bafilomycin
687 A1 Enhances NLRP3 Inflammasome Activation in Human Monocytes Independent of
688 Lysosomal Acidification." *The FEBS Journal* 288 (10): 3186–96.
689 https://doi.org/10.1111/febs.15619.
690 Zhang, Zhirong, Rossella Venditti, Li Ran, Zengzhen Liu, Karl Vivot, Annette Schürmann, Juan S.
691 Bonifacino, Maria Antonietta De Matteis, and Romeo Ricci. 2023. "Distinct Changes in
692 Endosomal Composition Promote NLRP3 Inflammasome Activation." *Nature*
693 *Immunology* 24 (1): 30–41. https://doi.org/10.1038/s41590-022-01355-3.
694 Zhu, Ping, Lihua Duan, Jie Chen, Ali Xiong, Qin Xu, Hongwei Zhang, Fang Zheng, Zheng Tan, Feili
695 Gong, and Min Fang. 2011. "Gene Silencing of NALP3 Protects Against Liver Ischemia–
696 Reperfusion Injury in Mice." *Human Gene Therapy* 22 (7): 853–64.
697 https://doi.org/10.1089/hum.2010.145.
698